LLNL-PROC-872252

PROCEEDINGS OF SCIENCE

Finite Temperature Transition in Hyper Stealth Dark Matter using Möbius Domain Wall Fermions

Venkitesh Ayyar,[a] Nobuyuki Matsumoto,[a] Aaron S. Meyer,[b,c] Sungwoo Park[b,c,*] and Lattice Strong Dynamics (LSD) collaboration

[a] *Hariri Institute for Computing and Computational Science and Engineering, Boston University, Boston, MA 02215, USA*

[b] *Physical and Life Sciences Division, Lawrence Livermore National Laboratory, Livermore, CA 94550, USA*

[c] *Nuclear Science Division, Lawrence Berkeley National Laboratory, Berkeley, CA 94720, USA*

E-mail: park49@llnl.gov

The first-order confinement transition of a strongly coupled composite dark matter theory can provide a possible source of gravitational waves in the early universe. In this work, on behalf of the Lattice Strong Dynamics (LSD) Collaboration, we present our recent investigation on the finite temperature confinement transition of the one-flavor SU(4) dark gauge theory named Hyper Stealth Dark Matter (HSDM). The dark matter candidate in this theory is a composite bosonic baryon and can have a remarkably low mass of a few GeV. We expect the finite temperature transition to be first-order over at least in some finite range of fermionic masses and to be a potential source of observable gravitational radiation. The finite temperature simulation of one-flavor SU(4) is done by using Möbius Domain wall fermions. The order of the transition and its fermionic mass dependence are explored by monitoring the Polyakov loop, chiral condensate and topological charge using three lattice volumes at $N_t = 8$.

The 41st International Symposium on Lattice Field Theory (LATTICE2024)
28 July - 3 August 2024
Liverpool, UK

*Speaker

PoS(LATTICE2024)148

1. Introduction

In recent years, the early universe has become a phenomenological laboratory to study new physics. In Ref. [1], the one-flavor SU(4) gauge theory was proposed as a model for the dark matter, which was named as the Hyper Stealth Dark Matter (HSDM). The dark matter candidate in this model is the lightest baryon composed of four dark-quarks, which can be as light as a few GeV. In the high-temperature phase of the universe, the HSDM is in a dark-quark-dark-gluon plasma, and as the universe cools down, the HSDM undergoes a phase transition into a confined phase of dark-hadrons. This phase transition, which is triggered by non-perturbative dynamics of the strongly-interacting theory, gives us another phenomenological interest as it can generate a stochastic background of gravitational waves if the transition is first-order [2] (see, e.g., [3, 4] for reviews; a possibility of detecting gravitational waves from crossover is also discussed [5]).

In this contribution, we study the confinement transition in the strongly-interacting SU(4) sector of this one-flavor model as a continuation of our previous report [6]. In particular, we determine the order of the phase transition with various dark-quark masses: $am \in \{0.01, 0.05, 0.1, 0.2, 0.3, 0.4, \infty\}$, including the quenched theory, $am = \infty$. We use the Wilson gauge action (with the conventional coupling β) and the Möbius Domain Wall Fermion (MDWF) [7, 8]. We used three lattice volumes $N_s^3 \times N_t$ with N_s =16, 24, and 32 at fixed $N_t = 8$ and $L_s = 16$. Gauge configurations are generated by the HMC with the exact one flavor algorithm (EOFA) [9]. Calculations are performed on LLNL clusters using Grid [10].

As is the case for the one-flavor theory with $N_c = 3$ [11], we expect the deconfinement transition to be first-order with heavy dark-quark masses and crossover with light dark-quark masses, separated by a second-order transition point. We study the critical coupling $\beta = \beta_{\rm crit}$ for various dark-quark masses by using the Polyakov loop as the order parameter. Note that, in the one-flavor theory, there is no spontaneous chiral symmetry breaking as $U_A(1)$ is broken explicitly by the chiral anomaly. Accordingly, the lightest meson η' acquires a mass of the order of the intrinsic scale of the theory, and it is expected to have no chiral phase transition [11, 12]. In this regard, we also investigate the chiral condensate and the topological charge around the confinement transition point $\beta_{\rm crit}$.

2. Möbius Domain Wall Fermion

As we have mentioned in the Introduction, the relation between chiral behavior and the deconfinement transition is of theoretical interest. In this study, we use the Möbius domain-wall fermion (MDWF) [7, 8] to systematically control the chiral symmetry breaking of the theory. As is well understood (see, e.g., Ref. [13] and reference therein), the breaking of the chiral symmetry due to finite L_s for domain-wall fermions can be quantified by the residual mass $m_{\rm res}$, which is related to the small eigenvalues of the hermitian Dirac operator: $H_4(M_5) = \gamma_5 \not{D}_W(-M_5)$, where M_5 is the domain-wall height. In this section, we briefly describe this residual breaking of the chiral symmetry in our ensembles.

Figure 1 shows the first ten smallest magnitude eigenvalues of $H_4(M_5)$ as a function of M_5 with the bare quark mass $am = 0.1$. We show results for the three representative cases with $am = 0.1$: $\beta = 10.6$, which corresponds to the deconfined phase; $\beta = 10.8$, around the critical point; and $\beta = 11.0$, the confined phase. The correspondence between β and the phases will be

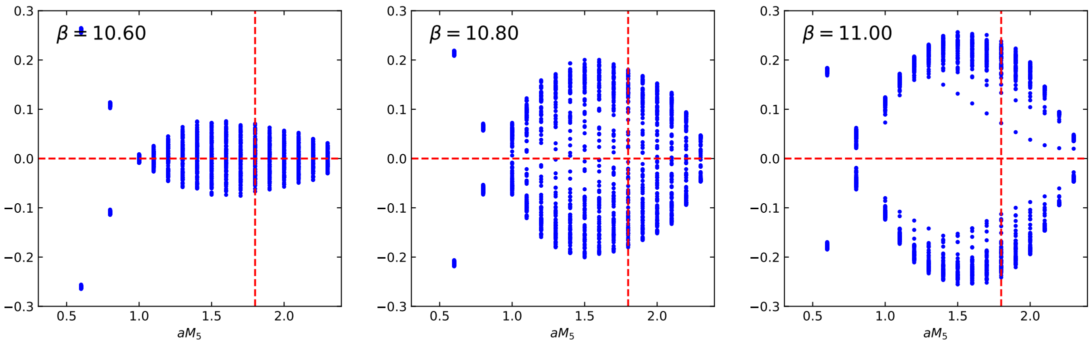

Figure 1: The ten smallest magnitude eigenvalues of the four-dimensional hermitian Dirac operator: $H_4(M_5) = \gamma_5 \not{D}_W(-M_5)$, calculated with ten thermalized configurations for $\beta = 10.6, 10.8, 11.0$ (from left to right) with the volume $24^3 \times 8$ and the bare quark mass $am = 0.1$. The red vertical dotted line indicates $aM_5 = 1.8$, which is the parameter used in the HMC for $am = 0.1$ and 0.4.

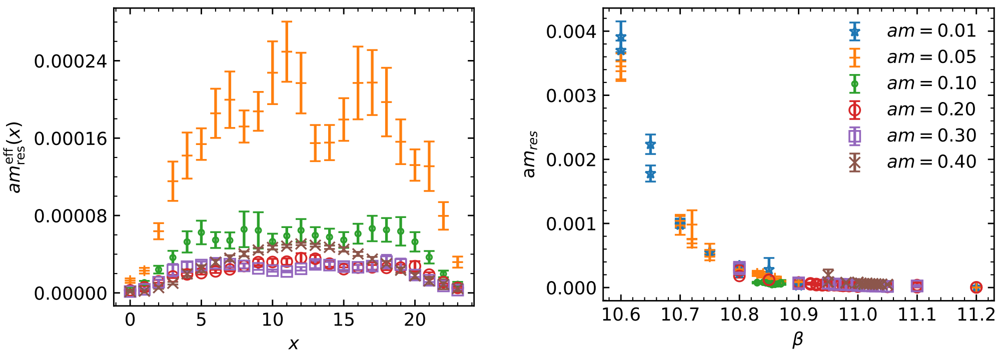

Figure 2: (Left) The effective residual mass $am^{\mathrm{eff}}_{\mathrm{res}}(x) = \langle J_{5q}(x)P(0)\rangle / \langle P(x)P(0)\rangle$ as a function of the spatial separation x, evaluated at β_{crit} for each quark mass. (Right) The residual mass m_{res} determined from the midpoint of $am^{\mathrm{eff}}_{\mathrm{res}}(x)$, plotted as a function of β. Both plots are calculated with the $24^3 \times 8$ ensembles.

given in Sec. 4. The red vertical line in the figure marks $M_5 = 1.8$, which is used in the HMC to generate the gauge configurations for $am = 0.1$ and 0.4. For simulations with other quark masses $am \in \{0.05, 0.2, 0.3\}$, we set $M_5 = 1.5$ to improve chiral behavior, based on Fig. 1. To further confirm that the breaking of the chiral symmetry according to finite L_s is well controlled, we calculate the residual mass from the axial Ward identity [14]: $m_{\mathrm{res}} = \lim_{x\to\infty} \langle J_{5q}(x)P(0)\rangle / \langle P(x)P(0)\rangle$, where P is the pseudoscalar meson operator and J_{5q} the five-dimensional flavor non-singlet axial current. In the left panel of Fig. 2, we show the effective residual mass $m^{\mathrm{eff}}_{\mathrm{res}}$ as a function of the spatial separation x for various quark masses at the critical coupling β_{crit} which will be determined in Sec. 4. The value of m_{res} is given at the midpoint. The effect of of the residual mass compared to the bare quark mass, m_{res}/m, is sub-percent for the parameters of interest and is therefore negligible.

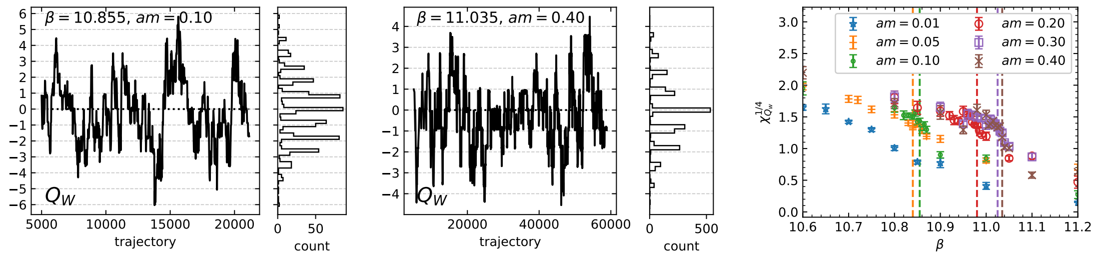

Figure 3: Monte Carlo time history of the Wilson-flowed topological charge Q_W, and the corresponding histogram calculated at β_{crit} for the masses: (left) $am = 0.1$ and (middle) $am = 0.4$. In the right panel, we show the topological susceptibility as a function of β for the six different quark masses: $m = 0.01, 0.05, 0.1, 0.2, 0.3, 0.4$. Vertical dotted lines are drawn at $\beta = \beta_{\text{crit}}$ to indicate the transition point for each mass with the same color used for the susceptibility.

3. Gauge ensemble

To ensure thermalization, we create two streams with a cold start from the unit gauge field ($U_\mu = 1$) and a hot start from a random gauge field for each β and the quark mass am. The sample size varies from 3000 to $O(10^5)$ (for the quenched case, up to $O(10^6)$), taking into account the diverging autocorrelation of the Polyakov loop and the topological charge. Figure 3 shows the Monte Carlo time history and the histogram of the Wilson-flowed topological charge Q_W, where we adopt the clover leaf definition for the field strength. The Wilson flow time is fixed to 2.0 with the step size 0.01. Though we see long autocorrelation, the sample size is large enough to observe a decent number of tunnelings in the ensemble, and as a result we obtain a symmetric distribution. With the current statistics, we do not observe a peak structure for the chiral susceptibility χ_{Q_W} (see the right-most panel in Fig. 3) around the critical coupling β_{crit}.

4. Deconfinement transition

We study the Polyakov loop (PL) as an order parameter for the deconfinement phase transition. Though the dynamical quark explicitly breaks the center symmetry, we expect it to still serve as an order parameter for large quark masses. Figure 4 shows the expectation value of the absolute value, $\langle|PL|\rangle$, as a function of β for various quark masses. The vanishing expectation values $\langle|PL|\rangle = 0$ at small β indicate the confined phase, while the nonzero values $\langle|PL|\rangle \neq 0$ at large β signify the deconfined phase. A diverging slope in the transition region in the infinite volume limit implies a phase transition.

To further discuss the phase transition, we plot in Fig. 5 the susceptibility of the Polyakov loop, which shows a peak structure at the transition region. The order of the phase transition can then be identified by studying the finite volume scaling of the height $\chi^{\text{max}}_{|PL|}$ of the peak, for which we make the ansatz: $\chi^{\text{max}}_{|PL|} \propto N_s^{3b}$. If the phase transition is first-order, the exponent b is expected to be 1 [15, 16]. Although the notion of the critical temperature is obscure when the transition is crossover, we write as β_{crit} the location of the peak in the susceptibility. As a preliminary study, we here determine the peak value $\chi^{\text{max}}_{|PL|}$ by fitting the bell-shaped peak in the Gaussian form. The obtained values for the exponent are $b = 0.46(10)$ for $am = 0.2$, $b = 0.49(19)$ for $am = 0.3$, $b = 1.02(19)$

PoS(LATTICE2024)148

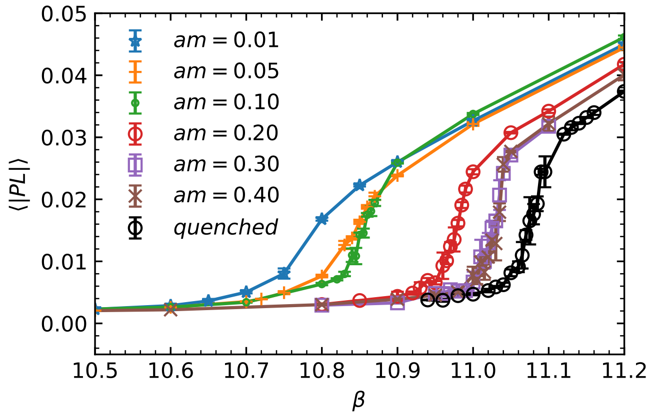

Figure 4: Polyakov Loop absolute value versus β on $24^3 \times 8$ ensembles.

for $am = 0.4$, and $b = 1.009(23)$ for the quenched theory. We do not use the results of $16^3 \times 8$ in estimating b for $am = 0.2, 0.3$ as it is deviates significantly from the scaling ansatz, in relation to which we can observe in Fig. 5 that $16^3 \times 8$ gives a significantly different value of β_{crit}.[1] for $16^3 \times 8$ with $am = 0.4$. Our analysis implies that the second-order point lies somewhere around $am = 0.3$ and 0.4. Most importantly, we find a finite dark-quark mass that is consistent with a first-order transition that can source gravitational waves.

It is interesting to see how the distribution of the Polyakov loop evolves across the phases. Figure 6 shows the scattered plot of the Polyakov loop in the complex plane before, in the middle of, and after the transition region, from left to right. In the quenched case (bottom row), where the Z_4 symmetry is preserved classically, we observe that the distribution of the Polyakov loop exhibits the Z_4 symmetry in the confined phase (bottom left) and it is broken spontaneously in the deconfinement phase (bottom right). Correspondingly, we observe $\langle PL \rangle = 0$ in the confined phase and $\langle PL \rangle \neq 0$ in the deconfined phase. With the dynamical dark-quarks (top and middle rows), where the Z_4 symmetry is explicitly broken, we see that the distribution in the confined phase is localized around zero (top/middle left), resulting in the expectation value $\langle PL \rangle = 0$. As we increase β, we observe a departure from the origin, moving towards the positive real axis (top/middle right), which we interpret as that the system has transited into the deconfined phase, giving $\langle PL \rangle \neq 0$.

To further scrutinize the transition, we look into the histogram. In Fig. 7, we plot the Monte Carlo time history and the histogram of $|PL|$ at β_{crit} for $m = 0.2$ (in the crossover region) and $m = 0.4$ (in the first-order region). Red and blue colors represent the hot and cold start streams, respectively. The first-order nature of the phase transition at $am = 0.4$ can be seen as the double-peaked structure in the histogram. We can further confirm the tendency that the separation between the two peaks becomes obscure as we decrease the dark-quark mass.

[1]We comment that the $16^3 \times 8$ ensembles shown in this figure are generated with $M_5 = 1.8$ while the $24^3 \times 8$ and $32^3 \times 8$ ensembles with $M_5 = 1.5$. While the parameters are to be unified, we expect the resulting difference in the observable to be small as described in Sec. 2.

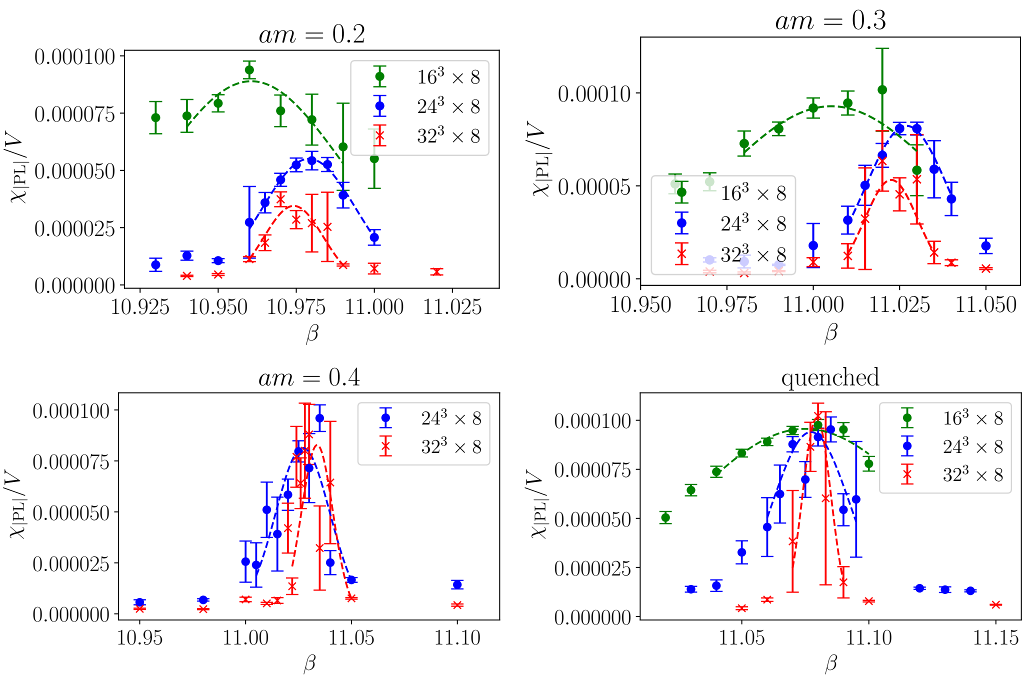

Figure 5: The Polyakov loop susceptibility normalized by the spatial volume, $\chi_{|\mathrm{PL}|}/V$, where $V = N_s^3$. Green, blue, and red points show the results for $16^3 \times 8$, $24^3 \times 8$, and $32^3 \times 8$, respectively. The ensembles with hot and cold starts are combined in this plot. As a preliminary study, the bell-shaped peaks are fitted in the Gaussian form, whose results are drawn with dashed lines. We see that the peak value of the susceptibility scales linearly with volume for $m = 0.4$ and the quenched case, signifying first-order phase transition.

5. Chiral susceptibility

As mentioned in the Introduction, the chiral symmetry is broken in the one-flavor theory by the axial anomaly. Consequently, unlike in QCD, chiral symmetry may not be restored in the large β limit. By using the chiral condensate $\langle\bar{\psi}\psi\rangle$ as the order parameter for the chiral phase transition, we can check this numerically in our model. The top three panels in Fig. 8 show the behavior of $\langle\bar{\psi}\psi\rangle$ around β_{crit} for the masses $am = 0.01, 0.2, 0.4$, drawn together with $\langle|PL|\rangle$ for comparison. We use a noisy estimator to calculate the condensate. It is interesting to observe a steep slope around β_{crit} even for $\langle\bar{\psi}\psi\rangle$. In the bottom three panels, we display the disconnected chiral susceptibility, $\chi_{\bar{\psi}\psi} = N_s^3 N_t (\langle(\bar{\psi}\psi)^2\rangle_{\mathrm{disc}} - \langle\bar{\psi}\psi\rangle^2)$, together with $\chi_{|PL|}$, in which the coincidental peak locations can be confirmed (especially for $am = 0.2$). Further study on their relative locations as well as the finite volume scaling for the chiral susceptibility are interesting in order to understand the non-perturbative dynamics of the theory. The study is in progress with improved statistics.

6. Conclusion and outlook

In this contribution, we gave an update from Ref. [6] on a strongly-interacting composite dark matter theory, the HSDM [1]; an SU(4) gauge theory with one flavor of Möbius domain-wall fermion. We explored the thermodynamics of this theory at various quark masses and β values by computing the topological charge, the Polyakov loop and the chiral condensate. We found that the

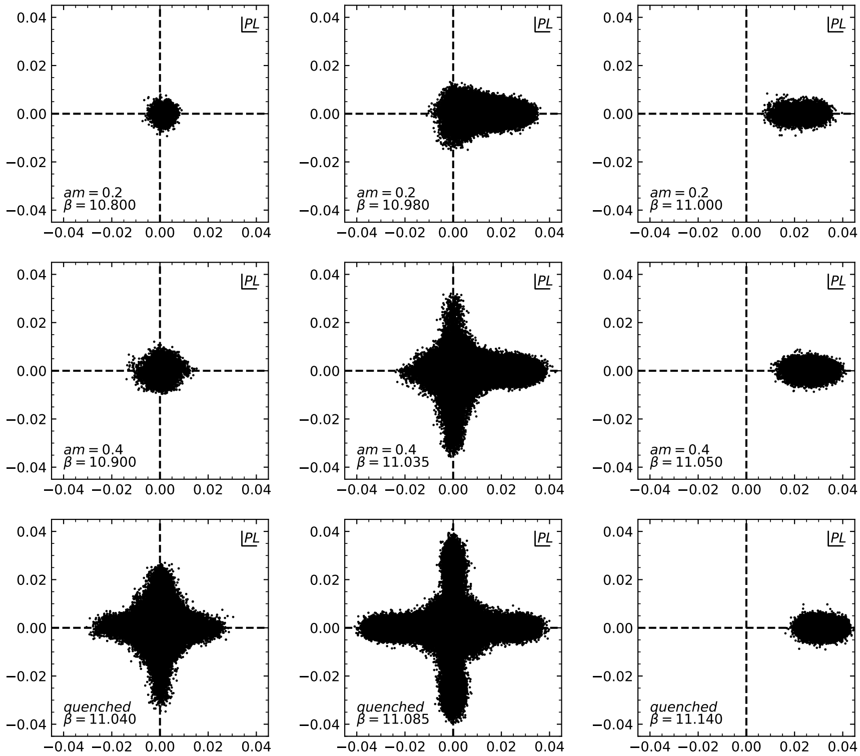

Figure 6: The scattered plot of the spatially averaged Polyakov loop in the complex plane for the masses $am = 0.2, 0.4$, and the quenched theory (from top to the bottom rows) on the $24^3 \times 8$ lattice. We choose three β values for each am: below, on top of, and above the coupling β_{crit} (from left to right).

transition is first-order at a large but moderate dynamical fermion mass. More detailed analysis with improved statistics is in progress, as well as zero temperature ensemble generation at β_{crit} for scale-setting in the theory by measuring the SU(4) meson and baryon masses.

Acknowledgments

This work was performed under the auspices of the U.S. Department of Energy by Lawrence Livermore National Laboratory under Contract DE-AC52-07NA27344. ASM is supported in part by Neutrino Theory Network Program Grant DE-AC02-07CHI11359, and U.S. Department of Energy Award DE-SC0020250. SP acknowledges the support from the ASC COSMON project. SP, ASM and P. M. Vranas would like to thank Scott Futral of LLNL for his support and early access to LLNL's exascale systems, Tuolumne and El Capitan where most of the numerical simulations were performed. NM is supported in part by the Scientific Discovery through Advanced Computing (SciDAC) program, "Multiscale acceleration: Powering future discoveries in High Energy Physics" under FOA LAB-2580 funded by DOE, Office of Science, and DOE under Award DE-SC0015845. Results presented in this contribution were produced using Grid [10].

PoS(LATTICE2024)148

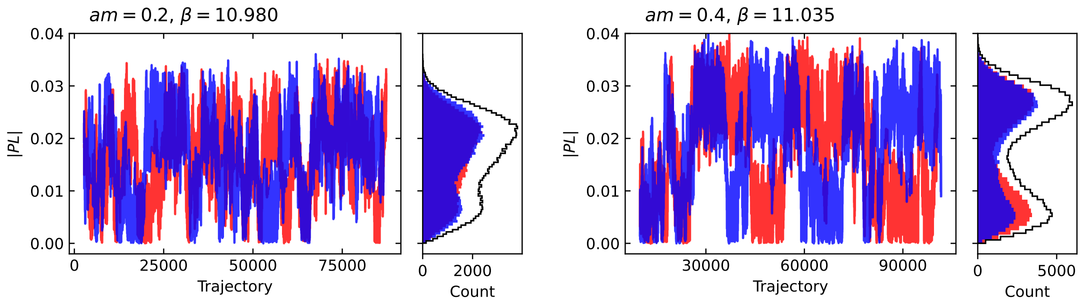

Figure 7: The Monte Carlo time history of the absolute value of the Polyakov loop, $|PL|$, and its histogram at $\beta_{\rm crit}$ for the masses below and above the second-order transition point: $am = 0.2, 0.4$ on the $24^3 \times 8$ lattice. The red and blue colors represent the hot and cold start streams, respectively, while the black curve shows the histogram that combines data from both streams.

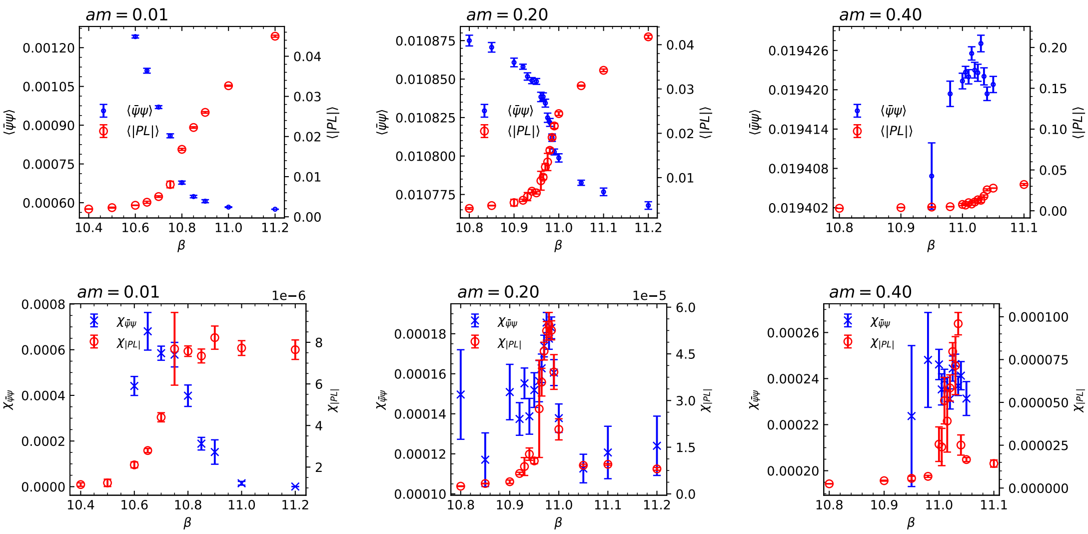

Figure 8: (Top) The chiral condensate and the Polyakov loop as a function of β. (Bottom) The disconnected chiral susceptibility and the Polyakov loop susceptibility as a function of β. The lattice size is fixed to $24^3 \times 8$ in this figure, while the dark-quark mass is varied as $am = 0.01, 0.2, 0.4$ from left to right.

References

[1] G.T. Fleming, G.D. Kribs, E.T. Neil, D. Schaich and P.M. Vranas, *Hyper Stealth Dark Matter and Long-Lived Particles*, 2412.14540.

[2] P. Schwaller, *Gravitational Waves from a Dark Phase Transition*, *Phys. Rev. Lett.* **115** (2015) 181101 [1504.07263].

[3] C. Caprini et al., *Detecting gravitational waves from cosmological phase transitions with LISA: an update*, *JCAP* **03** (2020) 024 [1910.13125].

[4] LISA Cosmology Working Group collaboration, *Cosmology with the Laser Interferometer Space Antenna*, *Living Rev. Rel.* **26** (2023) 5 [2204.05434].

[5] A. Escrivà, R. Inui, Y. Tada and C.-M. Yoo, *LISA forecast on a smooth crossover beyond the standard model through the scalar-induced gravitational waves*, *Phys. Rev. D* **111** (2025) 023528 [2404.12591].

[6] LSD collaboration, *Exploring Composite Dark Matter with an SU(4) gauge theory with 1 fermion flavor*, *PoS* **LATTICE2023** (2024) 102 [2402.07362].

[7] D.B. Kaplan, *A Method for simulating chiral fermions on the lattice*, *Phys. Lett. B* **288** (1992) 342 [hep-lat/9206013].

[8] R.C. Brower, H. Neff and K. Orginos, *The Möbius domain wall fermion algorithm*, *Comput. Phys. Commun.* **220** (2017) 1 [1206.5214].

[9] TWQCD collaboration, *Exact Pseudofermion Action for Monte Carlo Simulation of Domain-Wall Fermion*, *Phys. Lett. B* **738** (2014) 55 [1403.1683].

[10] P. Boyle, A. Yamaguchi, G. Cossu and A. Portelli, *Grid: A next generation data parallel C++ QCD library*, 1512.03487.

[11] C. Alexandrou, A. Borici, A. Feo, P. de Forcrand, A. Galli, F. Jegerlehner et al., *The Deconfinement phase transition in one flavor QCD*, *Phys. Rev. D* **60** (1999) 034504 [hep-lat/9811028].

[12] R.D. Pisarski and F. Wilczek, *Remarks on the Chiral Phase Transition in Chromodynamics*, *Phys. Rev. D* **29** (1984) 338.

[13] RBC, UKQCD collaboration, *Localization and chiral symmetry in three flavor domain wall QCD*, *Phys. Rev. D* **77** (2008) 014509 [0705.2340].

[14] CP-PACS collaboration, *Chiral properties of domain wall quarks in quenched QCD*, *Phys. Rev. D* **63** (2001) 114504 [hep-lat/0007014].

[15] K. Binder and D.P. Landau, *Finite-size scaling at first-order phase transitions*, *Phys. Rev. B* **30** (1984) 1477.

[16] M. Fukugita, M. Okawa and A. Ukawa, *Order of the Deconfining Phase Transition in SU(3) Lattice Gauge Theory*, *Phys. Rev. Lett.* **63** (1989) 1768.

PoS(LATTICE2024)148